Article:
Feng, Y., Qu, K., Yang, R. et al. (2026) Reversible broad-bias photoswitching of DNA molecular junctions via azobenzene-induced π-stack disruption. JACS Au. ISSN: 2691-3704

https://doi.org/10.1021/jacsau.6c00247

JACS Au
AN OPEN ACCESS JOURNAL OF THE AMERICAN CHEMICAL SOCIETY

pubs.acs.org/jacsau
Article

Reversible Broad-Bias Photoswitching of DNA Molecular Junctions via Azobenzene-Induced π-Stack Disruption

Yunxia Feng,[#] Kai Qu,[#] Ruiqi Yang, Nadav Amdursky, Ioan Bâldea,[*] and Zuoti Xie[*]

Cite This: https://doi.org/10.1021/jacsau.6c00247
Read Online

ABSTRACT: Reversible photoswitches that operate directly inside the DNA π-stack itself have remained elusive. Here, we introduce one or more azobenzene moieties into a DNA duplex while leaving the opposite position baseless. Reversible *trans-cis* photoisomerization strongly modulates longitudinal π-conjugation: the planar *trans* isomer partially preserves π-overlap across the defect, whereas the nonplanar *cis* isomer disrupts it dramatically. Both isomers substantially lower junction conductance compared to pristine DNA, but the *cis*-rich state induces a far more severe reduction. Conductive-probe atomic force microscopy reveals robustly reversible photoswitching: the *cis*-rich state lowers current by up to 2 orders of magnitude relative to the *trans*-rich state. On/off ratios increase superlinearly with the number of azobenzene units (up to ∼ 150 for three units) and remain >50 even at bias voltages of 1.5 V—exceptionally stable for a molecular photoswitch. Ultraviolet photoelectron spectroscopy confirms that the HOMO level of the DNA π-system is virtually unaffected both by azobenzene incorporation and by *trans-cis* isomerization. The observed switching therefore originates from a stronger suppressed rate of charge transfer across the *cis* defect, fully consistent with enhanced backscattering and possible destructive quantum interference due to its higher asymmetry location.

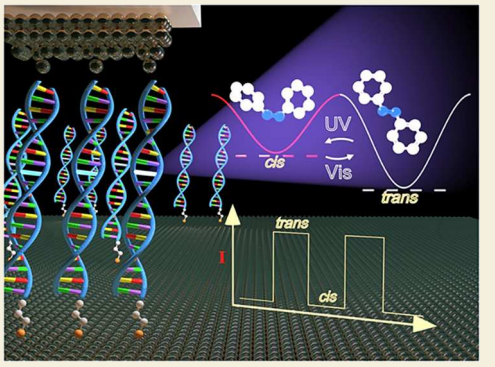

KEYWORDS: *molecular electronics, DNA junctions, azobenzene, photoswitching, π-stacking*

INTRODUCTION

DNA has attracted sustained interest in molecular electronics because its π-stacked nucleobases provide a natural one-dimensional pathway for charge migration along the helix axis.[1−8] Sequence-dependent π-overlap governs the dominant transport mechanism,[9−11] and even minor structural perturbations dramatically alter conductance.[4,12,13]

Out of many other photochromic molecules (e.g., diarylethene, stilbenes, spiropyrans, fulgides),[14−24] azobenzene is one of the most robust molecular photoswitches.[25] When tethered to D-threoninol, it has been widely used to photoregulate DNA hybridization and transcription by exploiting the large steric difference between the planar *trans* and bent *cis* isomers.[26,27] In those designs the azobenzene is inserted as an extra intercalator between intact base pairs, and switching relies primarily on *cis*-induced duplex dissociation rather than direct control of π-conjugation.

Despite various attempts, reversible photoswitches that operate inside the DNA π-stack itself—without breaking Watson−Crick base pairing—have remained elusive. Here we incorporate one or several (18-*n*A, *n* = 1, 2, 3) azobenzene moieties via D-threoninol linkers in an 18-base-pair duplex (Figures 1C,D, and S1). This embeds a genuine photoswitchable defect directly within the helical π-stack (Figure 1B). The planar *trans* isomer partially preserves π-overlap across the defect, whereas the strongly nonplanar *cis* isomer (phenyl rings twisted out of the original base-plane) dramatically disrupts longitudinal π-conjugation without dissociating the duplex.

Conductive-probe atomic force microscopy (CP-AFM) measurements on densely packed DNA monolayers (Figure 2A) reveal robust, reversible conductance photoswitching that persists up to bias voltages of ± 1.5 V (Figures 2 and S7). The *cis*-rich state lowers junction current by up to 2 orders of magnitude relative to the *trans*-rich state, with on/off ratios that rise superlinearly with the number of azobenzene units (Figure 3C).

Ultraviolet photoelectron spectroscopy (UPS) shows that the HOMO alignment of the DNA π-system remains virtually unchanged upon incorporation of either *trans*- or *cis*-azobenzene units relative to pristine DNA (18−0A) (Figures S9 and S6). Both isomers therefore act as defects that substantially lower junction conductance relative to pristine DNA, with the nonplanar *cis* form inducing a far stronger disruption. The additional orders-of-magnitude drop from

Received: February 17, 2026
Revised: April 1, 2026
Accepted: April 3, 2026

https://doi.org/10.1021/jacsau.6c00247
JACS Au XXXX, XXX, XXX−XXX

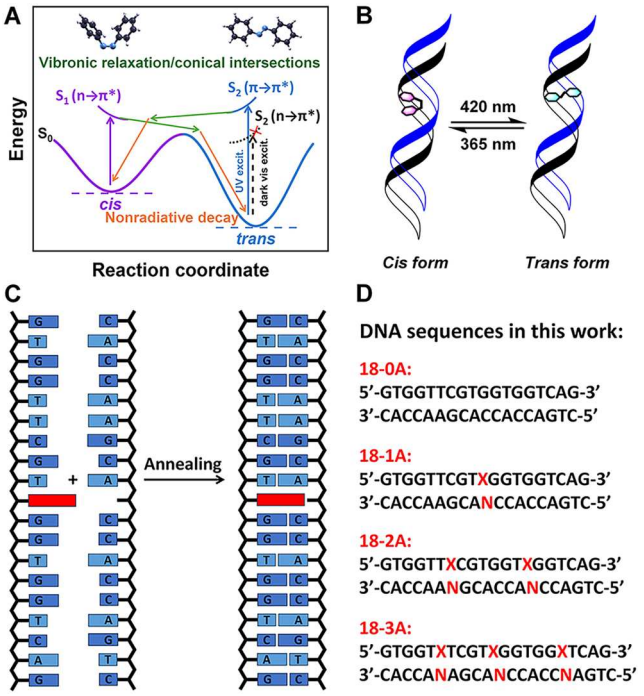

Figure 1. Schematic representation of *cis*⇋*trans* photoisomerization of (A) the isolated azobenzene molecule (see Supporting Information for details) and (B) incorporated into the DNA helix. (C) Schematic illustration of duplex design of 18−1A. One azobenzene moiety is site-specifically inserted into the middle of the helix via D-threoninol on one strand while the opposing strand carries an abasic site (no nucleobase). (D) Sequence design of the azobenzene-tethered DNA. "X" represents an azobenzene moiety while "N" indicates either no base or modification on sugar−phosphate backbone at the corresponding position.

trans-rich to *cis*-rich states thus reflects a strongly suppressed rate of charge transfer across the azobenzene-induced defect in the π-stack — fully consistent with enhanced backscattering of the propagating hole wave and possible destructive quantum interference arising from the asymmetric placement of the defect.

To our knowledge, this is the first demonstration of broad-bias, reversible photoswitching in DNA molecular junctions achieved by direct manipulation of the native π-stack continuity itself.

RESULTS AND DISCUSSION

Growth and Characterization of DNA Sequence

We designed an 18-base-pair DNA sequence (Figure 1C,D) and introduced azobenzene moieties into one strand using D-threoninol as a linker (Figure S1). After annealing, we obtained double-stranded DNA with site-specific azobenzene modifications (Figure 1C). Notably, unlike previously reported intercalation approaches in synthetic biology,[26,27] which incorporate azobenzene into the narrow gap between two intact DNA bases, we simultaneously inserted a sugar moiety without a nucleobase at the corresponding position in the complementary strand (Figures 1C,D, and S1). Our strategy did not aim to dissociate the duplex via steric hindrance from the *cis* isomer,[26,27] but to allow the planar *trans*-azobenzene to maintain partial π-conjugation with adjacent bases while providing sufficient space for *cis*-configurational switching without disrupting Watson−Crick hydrogen bonding. Although the nonideal planarity of azobenzene partially perturbed the helical structure, the modified DNA still retained partial B-form chirality (see circular dichroism spectra in Figure S4 and details in the Supporting Information).

The sequences studied in this work comprised pristine DNA (18−0A) and variants containing one, two, or three azobenzene units (18−1A, 18−2A, and 18−3A), as illustrated in Figures 1B and S1.

UV−vis spectroscopy confirmed efficient photoswitching of the azobenzene-modified DNA in solution[25] (Figures S2 and S3; mechanistic details are provided in Supporting Information). Irradiation at 365 nm drove *trans*-to-*cis* isomerization, whereas 420 nm light induced the reverse *cis*-to-*trans* process (Figure 1B). No further spectral changes were observed after 30 min of irradiation, indicating that a photostationary state had been reached. Pristine DNA (18−0A) showed no response to either wavelength.

To enable covalent attachment to gold substrates, the oligonucleotides were functionalized with a 3′-C3 thiol linker. Self-assembly of the DNA on template-stripped gold surfaces produced well-oriented monolayers, as confirmed by X-ray photoelectron spectroscopy (XPS). As shown in Figure S5, the C 1s, N 1s, and P 2p peak intensities increased progressively with the number of azobenzene units, whereas the S 2p intensity remained constant and the Au 4f signal decreased. The C 1s/S 2p integrated intensity ratio rose linearly with the number of azobenzene modifications (Figure S5F) consistent with upright-oriented DNA strands bound via thiol−gold

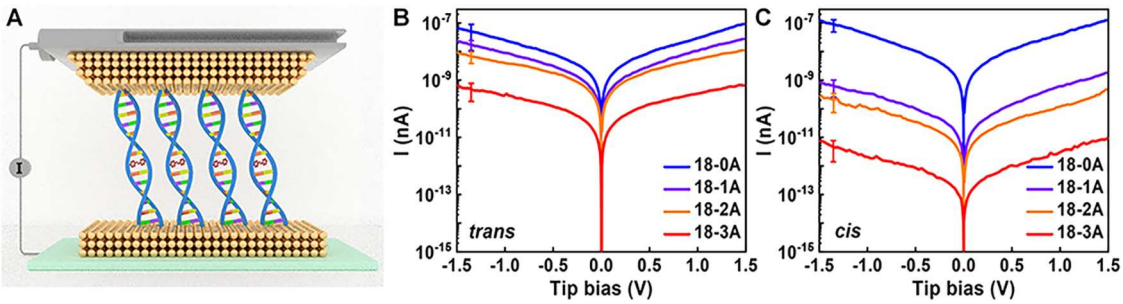

Figure 2. (A) Schematic representation of the CP-AFM setup. Semilog plots of average *I*−*V* curves of DNA junctions after prior exposure to (B) visible (*trans*-states) and (C) UV light (*cis*-states). Error bars represent one standard deviation based on 150−250 *I*−*V* curves measured per sample after each illumination condition.

https://doi.org/10.1021/jacsau.6c00247
JACS Au XXXX, XXX, XXX−XXX

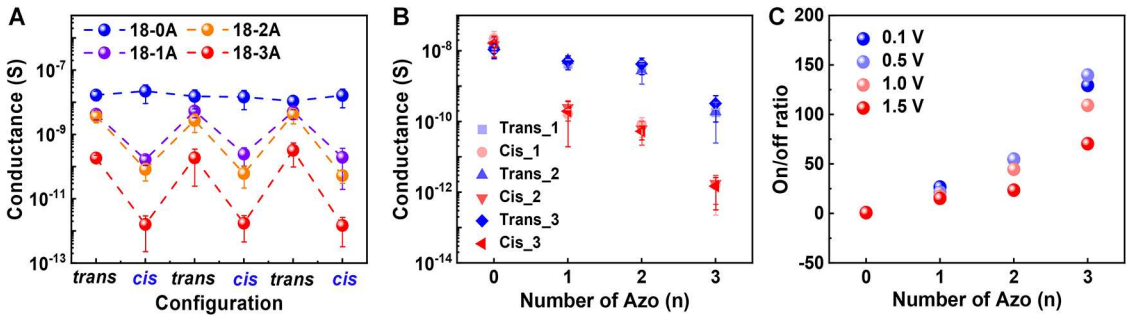

Figure 3. (A) Low bias conductance reversibly switching between high and low values after three consecutive exposures to visible (vis) and ultraviolet (uv) radiation. (B) Conductance of junctions with variable number of *trans* (blue) and *cis* (red) azobenzene incorporations. (C) On/off ratio of the measured over three cycles for junctions with different number of azobenzene insertions at several biases. Error bars represent one standard deviation based on 150−250 $I-V$ curves measured per sample after each illumination condition. Notice that the on/off ratio remains significantly larger than unity up to biases as high as 1.5 V. The superlinear dependence of the on/off ratio on the number of azobenzene insertions is the direct consequence of the different *trans* and *cis* conductance's attenuation coefficient β. Low-bias conductance decreases exponentially with the number of azobenzene units in each isomeric state (panel B), yielding distinct attenuation coefficients ($\beta_{trans} \approx 0.85$/azobenzene, $\beta_{cis} \approx 2.3$/azobenzene).

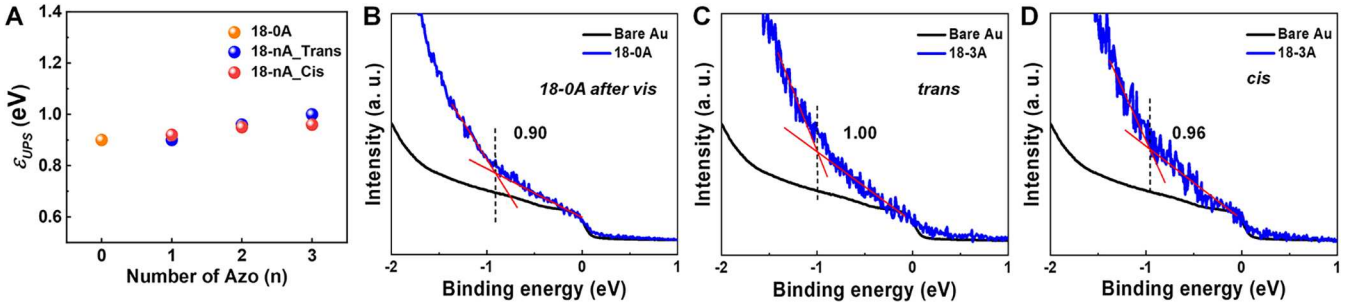

Figure 4. (A) The HOMO energy offset for SAMs fabricated with pristine (18−0A) DNA, and with a variable number of *trans* and *cis* azobenzene incorporations measured via UPS. UPS spectra for several constructs: (B) pristine 18−0A, (C) *trans*18−3A and (D) *cis*18−3A. (Additional UPS spectra in Figure S6).

linkages rather than lying flat on the surface due to nonspecific physisorption through phosphate or nucleobase groups.[28,29]

Electrical Characterization

The electrical conductance of the DNA SAM was measured using CP-AFM,[30−32] as illustrated in Figure 2A. Au-coated probe tips were placed in soft contact (∼1 nN compression) with the DNA films, and current−voltage ($I-V$) characteristics were acquired by sweeping the bias at the tip while maintaining the substrate grounded.

We exposed the self-assembled monolayer (SAM) to focused ultraviolet light (365 nm) and visible light (420 nm) at a fixed distance for 30 min, while maintaining the sample temperature at 5−10 °C to minimize heat-induced effects on the sample and the azobenzene configuration. The ambient relative humidity was controlled and kept at 60% to ensure the sample surface remained moist throughout the illumination process. After light exposure, the sample was dried with nitrogen gas, and current−voltage ($I-V$) measurements were conducted using CP-AFM within 2 h under dark conditions. Figure 2B and C show the $I-V$ curves of the SAM after ultraviolet and visible light exposure, respectively, plotted on a semilogarithmic scale. No significant change in current was observed in the 18−0A system after either light treatment. In contrast, samples 18−1A, 2A, and 3A exhibited decreased conductivity following UV irradiation.

The difference in conductance and currents at several biases before and after light exposure is reported in Figure 3, which collects the central findings of the present work. Figure 3A demonstrates that the light-induced change in conductance is substantial and reproducible. We compared the conductance of the DNA molecular junctions with the number of incorporated azobenzene units (Figure 3B). Within each isomeric state, the low-bias conductance decreases exponentially with the number of incorporated azobenzene units, with distinct attenuation coefficients ($\beta_{trans} \approx 0.85$ and $\beta_{cis} \approx 2.3$ per azobenzene). We attribute this effect to the disruption of $\pi-\pi$ stacking within DNA by both *trans*- and *cis*-azobenzene, with the *cis*-configuration having a stronger impact than the *trans*-configuration, thereby leading to the observed changes in conductance.

Figure 3C presents the on/off ratio of conductance and currents at several biases before and after illumination. Junctions with pristine DNA (i.e., without azobenzene) showed a ratio close to unity (no switching), while those with more azobenzene modifications exhibited higher switching ratios. Even at bias voltages as high as 1.5 V, the on/off ratio remains greater than 50 for the triple-azobenzene construct 18−3A and reaches approximately 150 at low bias—exceptionally stable performance for a molecular photoswitch reported to date.[23]

The persistence of high on/off ratios up to ± 1.5 V is particularly significant because many molecular photoswitches exhibit diminished contrast at elevated bias due to bias-induced flattening of the transmission function or the onset of competing transport channels. Moreover, operation at such voltages tests the electrochemical stability of both the

https://doi.org/10.1021/jacsau.6c00247
JACS Au XXXX, XXX, XXX−XXX

azobenzene switch and the DNA junction itself. The robust performance observed here demonstrates that the azobenzene-modified DNA constructs withstand substantial electric fields without degradation or loss of switching functionality, underscoring the potential of this platform for integration into optoelectronic devices requiring stable operation over a wide bias range.

Interpretation

In DNA-based molecular junctions, hole transport through the π-stack dominates the current.[4,33,34] Regardless of the specific theoretical framework used to describe charge transport the measured conductance is fundamentally determined by two factors: (1) the energetic alignment $|\varepsilon_0|$ of the relevant frontier orbital (HOMO) with the electrode Fermi level, and (2) the effective rate Γ at which charge carriers cross the molecule−electrode interfaces and propagate through the DNA wire.

UPS unambiguously shows that ε_0 is virtually unaffected (variation ∼ 0.1 eV or 10%) both by the incorporation of one to three azobenzene units and by *trans* ⇌ *cis* photoisomerization (Figure 4A). All these differences in ε_0 are comparable with typical statistical deviations not only for the present junctions but also for other benchmark CP-AFM junctions ranging from those based on aromatic molecules possessing delocalized π-electrons[31] or saturated alkyl chains with localized σ-electrons.[32] A change of this magnitude can alter conductance by at most ∼20% eq (S2), far too small to explain the observed drop of up to 2 orders of magnitude upon UV irradiation.

Consequently, the dramatic and reversible photoswitching can only arise from a strong modulation of the charge-transfer rate Γ. This is understandable microscopically. Γ quantifies the rate of charge transfer between holes of the HOMO delocalized over the DNA strands and electrodes. Defects act as (back)scatterers.

Trans-azobenzene enables partial π-overlap (moderate backscattering, moderate Γ reduction with respect to the pristine 18−0A) while *cis* breaks it (strong reflection, like a one-dimensional barrier, Γ reduction significantly stronger than that for *trans* incorporations). Asymmetric placement (azobenzene vs abasic) may add *cis*-state destructive interference between strands. Each additional azobenzene unit multiplies this backscattering effect, leading to the observed superlinear increase in the on/off ratio with the number of defects (Figure 3C).

This interpretation is completely general and does not rely on any particular transport model. Still, for completeness we note that all individual $I-V$ curves—for pristine DNA as well as for *trans*-rich and *cis*-rich 18-nA (n = 1, 2, 3) junctions—can be accurately reproduced using the off-resonant single-level model (Figure S7),[35] which yields ε_0 values fully consistent with the UPS results (Figure S9A and B). The quantitative agreement merely corroborates the qualitative, model-independent conclusion: photoswitching is almost exclusively Γ-driven (Figure S9C).

CONCLUSION

We have demonstrated a fundamentally new strategy for embedding genuine, reversible photoswitchable defects directly within the native π-stack of duplex DNA. By inserting one or more central A−T base pairs with an azobenzene moiety tethered via D-threoninol on one strand and deliberately introducing an abasic site on the opposing strand, we created a light-responsive interruption of the helical π-system without relying on duplex dissociation. The planar *trans*-azobenzene partially maintains longitudinal π-conjugation, whereas the strongly nonplanar *cis* isomer disrupts it dramatically, leading to a pronounced and reversible modulation of hole transport along the DNA bridge.

Conductive-probe AFM measurements on densely packed, thiol-anchored DNA monolayers reveal exceptionally robust conductance photoswitching: on/off ratios increase superlinearly with the number of azobenzene units, reaching approximately 150 at low bias and remaining greater than 50 even at 1.5 V for the triple-substituted construct (18−3A) — performance that is remarkable among molecular photoswitches and persists over multiple switching cycles without fatigue.

The observed switching originates almost exclusively from a light-induced collapse of the effective charge-transfer rate across the defect(s), driven by strongly enhanced hole backscattering and possible destructive quantum interference in the *cis* configuration.

To our knowledge, this is the first example of a DNA-based optoelectronic switch in which conductance is controlled predominantly by direct, reversible manipulation of the continuity of the native π-stack itself, rather than by orbital energy shifts, molecular length changes, or hybridization-state melting. The approach establishes a versatile platform for introducing functional, non-natural defects into biomolecular electronic circuits and opens new avenues toward light-programmable bioelectronic interfaces, dynamic DNA nanomachines, and sequence-defined optoelectronic materials.

MATERIALS AND METHODS

Materials

All metals were purchased from Kurt J. Lesker Co. Silicon (100) wafers were obtained from Wafer Net (Prmat, Shangai, China). Contact mode AFM tips (DNP silicon nitride probes) were purchased from Bruker AFM Probes. The disodium phosphate, monosodium phosphate, and magnesium chloride, disodium chloride, tris (2-carboxyethyl) phosphine (TCEP) used in this study was purchased from Sigma-Aldrich. All DNA oligonucleotides were synthesized by and purchased from Sangon Biotech.

UV−vis Spectroscopy

Photoisomerization of the 18-nA constructs was monitored using an Agilent Cary 300 UV−vis spectrophotometer at room temperature. Samples (25 μM in PBS buffer) were first irradiated with 420 nm visible light from a 16 W LED lamp for 30 min to enrich the *trans* isomer and remove any residual *cis* contamination. Absorption spectra were then recorded from 550 to 200 nm. Immediately thereafter, the same solution was irradiated with 365 nm UV light from a 16 W LED lamp for 30 min to drive *trans*-to-*cis* conversion. To suppress thermal *cis*-to-*trans* reversion and prevent thermally induced duplex unwinding, the sample was maintained in a cold-water bath at 5−10 °C during UV exposure. The absorption spectrum was subsequently recorded again over the same wavelength range using identical instrument settings. Pristine DNA (18−0A) served as a control and showed no spectral changes upon irradiation.

Conducting Tip and Sample Preparation

Conductive AFM tips used for current measurements were prepared by coating Au at a base pressure of 10^{-7} Torr using a thermal evaporator placed in a N_2-filled glovebox. Au was deposited to a thickness of 50 nm at a rate of 0.1 Å/s with a ∼5 nm Cr adhesion layer. They were immediately transferred to another N_2-filled glovebox to carry out the $I-V$ measurements without exposure to air. The radius of the Au coated AFM tip is expected to be ∼50 nm.

https://doi.org/10.1021/jacsau.6c00247
JACS Au XXXX, XXX, XXX−XXX

For template-stripped flat Au substrates, 200 nm of Au was directly deposited onto clean Si wafers in a high vacuum e-beam evaporator. We then glued Si chips (~1 cm^{-2}) onto the metal surface using epoxy. The epoxy layer was cured by placing the wafers in an oven at 150 °C for 1 h. To form double-stranded DNA duplexes (-dsDNA), we did stepwise annealing for the hybridization of ssDNA using PCR thermal incubation. Before absorption, the dimers were treated with 10 mM TCEP (tris(2-carboxyethyl) phosphine hydrochloride) in 0.05 M PBS (pH 7.0, Na_2HPO_4, NaH_2PO_4, with 0.01 M $MgCl_2$ and NaCl) for 2 h to reduce the disulfide bond to the thiol bond. The mixture was then purified by filtering through a Micro Bio-Spin P-30 column and finally was diluted into 50 μM solution with 0.05 M PBS buffer. The dimer solution was then dropped on the Au surface of template substrates. The solution was left on the surface overnight at room temperature in a controlled-humidity environment. After this, the samples were washed with PBS and deionized water to eliminate any excess DNA and salts before they were dried using N_2 gas.

Transport Measurements

Current−voltage measurements were completed by mounting the substrates in the AFM and bringing the metal-coated tip into contact with the SAM under ~1 nN of the applied compressive load. Voltages were applied to the tip with a Keithley model 236 source-measure unit operated in "DC mode". Voltage was swept at the tip, the sample was grounded, and current−voltage characteristics were recorded. The slope of the linear portion of the $I-V$ characteristic was used to define a junction (low bias) conductance G. To observe the pronounced nonlinear ($I-V$) behavior, voltage sweeps to ± 1.5 V for all the samples.

To assess reversible photoswitching, each junction underwent three consecutive measurement cycles. In each cycle, the sample was first irradiated with 420 nm visible light for 30 min at 5−10 °C to enrich the *trans* state, followed by an $I-V$ measurement. It was then irradiated with 365 nm UV light under the same cooling conditions to enrich the *cis* state, followed by another measurement. Throughout all illumination steps, the sample was placed on a cooled surface to minimize thermal effects. Due to controlled ambient humidity, a thin water film condensed on the cooled surface during illumination; this residual moisture was removed prior to electrical measurements using a gentle nitrogen flow and brief evacuation. The resulting conductance values are labeled "*trans*1, *cis*1, *trans*2, *cis*2, *trans*3, *cis*3" (see Figure 3B). All measurements were conducted in a dark environment with the AFM's internal light source switched off to prevent unintended photoisomerization or interference.

■ ASSOCIATED CONTENT

Supporting Information

The Supporting Information is available free of charge at https://pubs.acs.org/doi/10.1021/jacsau.6c00247.

Molecular structures (Figure S1); UV−vis and CD spectra (Figures S2−S4); XPS and UPS data (Figures S5−S6); $I-V$ curves and transport fits (Figures S7−S9); conductance table (Table S1); photoisomerization mechanism; and experimental methods (PDF)

■ AUTHOR INFORMATION

Corresponding Authors

Ioan Bâldea − *Theoretical Chemistry, Heidelberg University, D-69120 Heidelberg, Germany;* orcid.org/0000-0003-4860-5757; Email: ioan.baldea@pci.uni-heidelberg.de

Zuoti Xie − *Department of Materials Science and Engineering, MATEC, Guangdong Technion-Israel Institute of Technology, Shantou, Guangdong 515063, China; Quantum Science Center of Guangdong-Hong Kong-Macao Greater Bay Area (Guangdong), Shenzhen-Hong Kong International Science and Technology Park, Shenzhen, Guangdong 518000, China;* orcid.org/0000-0002-1828-0122; Email: zuoti.xie@gtiit.edu.cn

Authors

Yunxia Feng − *Department of Materials Science and Engineering, MATEC, Guangdong Technion-Israel Institute of Technology, Shantou, Guangdong 515063, China; Schulich Faculty of Chemistry, Technion-Israel Institute of Technology, Haifa 3200003, Israel;* orcid.org/0009-0007-6229-6483

Kai Qu − *Department of Materials Science and Engineering, MATEC, Guangdong Technion-Israel Institute of Technology, Shantou, Guangdong 515063, China*

Ruiqi Yang − *Department of Materials Science and Engineering, MATEC, Guangdong Technion-Israel Institute of Technology, Shantou, Guangdong 515063, China*

Nadav Amdursky − *Schulich Faculty of Chemistry, Technion-Israel Institute of Technology, Haifa 3200003, Israel; Chemistry, School of Mathematical and Physical Sciences, University of Sheffield, Sheffield S3 7HF, U.K.;* orcid.org/0000-0003-1543-5333

Complete contact information is available at: https://pubs.acs.org/10.1021/jacsau.6c00247

Author Contributions

#Y.F. and K.Q. contributed equally to this work.

Notes

The authors declare no competing financial interest.

■ ACKNOWLEDGMENTS

Z.X. acknowledges primary financial support from the National Key R&D Program of China (2023YFA1407100) and the National Natural Science Foundation of China (22373026) and Guangdong Science and Technology Department (2021B0301030005, STKJ2023072, GDZX2304005, GDZX2504001, and 2021QN02×538). I.B. gratefully acknowledges computational support by the state of Baden-Württemberg through bwHPC and the German Research Foundation through Grant Nos. INST 40/575-1, 35/1597-1, and 35/1134-1 (JUSTUS 2, bwUniCluster 2/3, and bwForCluster/MLS&WISO/HELIX 2).

■ REFERENCES

(1) Porath, D.; Bezryadin, A.; de Vries, S.; Dekker, C. Direct Measurement of Electrical Transport through DNA Molecules. *Nature* **2000**, *403*, 635−638.

(2) Grozema, F. C.; Siebbeles, L. D. A.; Berlin, Y. A.; Ratner, M. A. Hole Mobility in DNA: Effects of Static and Dynamic Structural Fluctuations. *ChemPhysChem* **2002**, *3*, 536−539.

(3) Endres, R. G.; Cox, D. L.; Singh, R. R. P. Colloquium: The Quest for High-Conductance DNA. *Rev. Mod. Phys.* **2004**, *76*, 195−214.

(4) Xiang, L.; Palma, J. L.; Bruot, C.; Mujica, V.; Ratner, M. A.; Tao, N. Intermediate Tunnelling-Hopping Regime in DNA Charge Transport. *Nat. Chem.* **2015**, *7*, 221−226.

(5) Xiang, L.; Palma, J. L.; Li, Y.; Mujica, V.; Ratner, M. A.; Tao, N. Gate-controlled conductance switching in DNA. *Nat. Commun.* **2017**, *8*, No. 14471, DOI: 10.1038/ncomms14471.

(6) Guo, C.; Wang, K.; Zerah-Harush, E.; Hamill, J.; Wang, B.; Dubi, Y.; Xu, B. Molecular Rectifier Composed of DNA with High Rectification Ratio Enabled by Intercalation. *Nat. Chem.* **2016**, *8*, 484−490.

(7) Zhang, D.; Feng, Y.; Xu, X.; Jia, K.; Emusani, R.; Zhang, Z.-Y.; Zhang, J.; Zuo, X.; Zhao, Z.; Li, T.; Ma, L.; Xiang, D. Reversing the Conductance Evolution of Azobenzene Derivatives in Photoisomerization. *Phys. Rev. Lett.* **2025**, *135*, No. 218001.
(8) Zhang, Y.; Li, T. Modular One-pot Construction of Solar Azoswitches Based on Heteroaryl Organozinc Reagents. *J. Am. Chem. Soc.* **2025**, *147*, 42024−42031.
(9) Zhang, Y.; Liu, C.; Balaeff, A.; Skourtis, S. S.; Beratan, D. N. Biological charge transfer via flickering resonance. *Proc. Natl. Acad. Sci. U.S.A.* **2014**, *111*, 10049−10054.
(10) Nano, A.; Furst, A. L.; Hill, M. G.; Barton, J. K. DNA Electrochemistry: Charge-Transport Pathways through DNA Films on Gold. *J. Am. Chem. Soc.* **2021**, *143*, 11631−11640.
(11) Mishra, S.; Poonia, V. S.; Fontanesi, C.; Naaman, R.; Fleming, A. M.; Burrows, C. J. Effect of Oxidative Damage on Charge and Spin Transport in DNA. *J. Am. Chem. Soc.* **2019**, *141*, 123−126.
(12) Wang, K.; Hamill, J. M.; Wang, B.; Guo, C.; Jiang, S.; Huang, Z.; Xu, B. Structure determined charge transport in single DNA molecule break junctions. *Chem. Sci.* **2014**, *5*, 3425−3431.
(13) Zhuravel, R.; Huang, H.; Polycarpou, G.; Polydorides, S.; Motamarri, P.; Katrivas, L.; Rotem, D.; Sperling, J.; Zotti, L. A.; Kotlyar, A. B.; Cuevas, J. C.; Gavini, V.; Skourtis, S. S.; Porath, D. Backbone charge transport in double-stranded DNA. *Nat. Nanotechnol.* **2020**, *15*, 836−840.
(14) Zhang, J.; Whitesell, J. K.; Fox, M. A. Photoreactivity of Self-assembled Monolayers of Azobenzene or Stilbene Derivatives Capped on Colloidal Gold Clusters. *Chem. Mater.* **2001**, *13*, 2323−2331.
(15) Dulić, D.; van der Molen, S. J.; Kudernac, T.; Jonkman, H. T.; de Jong, J. J. D.; Bowden, T. N.; van Esch, J.; Feringa, B. L.; van Wees, B. J. One-Way Optoelectronic Switching of Photochromic Molecules on Gold. *Phys. Rev. Lett.* **2003**, *91*, No. 207402.
(16) Fuß, W.; Constantine, K.; Schmid, W. E.; Trushin, S. A. The Photochemical cis-trans Isomerization of Free Stilbene Molecules Follows a Hula-Twist Pathway. *Angew. Chem., Int. Ed.* **2004**, *43*, 4178−4182.
(17) Chen, Y.; Wang, C.; Fan, M.; Yao, B.; Menker, N. Photochromic fulgide for holographic recording. *Opt. Mater.* **2004**, *26*, 75−77.
(18) Li, J.; Speyer, G.; Sankey, O. F. Conduction Switching of Photochromic Molecules. *Phys. Rev. Lett.* **2004**, *93*, No. 248302.
(19) Heinz, B.; Malkmus, S.; Laimgruber, S.; Dietrich, S.; Schulz, C.; Rück-Braun, K.; Braun, M.; Zinth, W.; Gilch, P. Comparing a Photoinduced Pericyclic Ring Opening and Closure: Differences in the Excited State Pathways. *J. Am. Chem. Soc.* **2007**, *129*, 8577−8584.
(20) del Valle, M.; Gutiérre, R.; Tejedor, C.; Cuniberti, G. Tuning the Conductance of a Molecular Switch. *Nat. Nano* **2007**, *2*, 176−179.
(21) Uchida, K.; Yamanoi, Y.; Yonezawa, T.; Nishihara, H. Reversible On/Off Conductance Switching of Single Diarylethene Immobilized on a Silicon Surface. *J. Am. Chem. Soc.* **2011**, *133*, 9239−9241.
(22) Lenfant, S. *Molecular Electronics: An Experimental and Theoretical Approach*; Bâldea, I., Ed.; Pan Stanford: Singapore, 2015; pp 65−99.
(23) Jia, C.; Migliore, A.; Xin, N.; et al. Covalently Bonded Single-Molecule Junctions with Stable and Reversible Photoswitched Conductivity. *Science* **2016**, *352*, 1443−1445.
(24) Taherinia, D.; Frisbie, C. D. Photoswitchable Hopping Transport in Molecular Wires 4 nm in Length. *J. Phys. Chem. C* **2016**, *120*, 6442−6449.
(25) Bandara, H. M. D.; Burdette, S. C. Photoisomerization in different classes of azobenzene. *Chem. Soc. Rev.* **2012**, *41*, 1809−1825.
(26) Asanuma, H.; Liang, X.; Nishioka, H.; Matsunaga, D.; Liu, M.; Komiyama, M. Synthesis of azobenzene-tethered DNA for reversible photo-regulation of DNA functions: hybridization and transcription. *Nat. Protoc.* **2007**, *2*, 203−212.
(27) Kamiya, Y.; Asanuma, H. Light-driven DNA nanomachine with a photoresponsive molecular engine. *Acc. Chem. Res.* **2014**, *47*, 1663−1672.
(28) Xiao, P. F.; Cheng, L.; Wan, Y.; Sun, B. L.; Chen, Z. Z.; Zhang, S. Y.; Zhang, C. Z.; Zhou, G. H.; Lu, Z. H. An improved gel-based DNA microarray method for detecting single nucleotide mismatch. *Electrophoresis* **2006**, *27*, 3904−3915.
(29) Aqua, T.; Naaman, R.; Daube, S. S. Controlling the Adsorption and Reactivity of Dna on Gold. *Langmuir* **2003**, *19*, 10573−10580.
(30) Xie, Z.; Bâldea, I.; Demissie, A. T.; Smith, C. E.; Wu, Y.; Haugstad, G.; Frisbie, C. D. Exceptionally Small Statistical Variations in the Transport Properties of Metal-Molecule-Metal Junctions Composed of 80 Oligophenylene Dithiol Molecules. *J. Am. Chem. Soc.* **2017**, *139*, 5696−5699.
(31) Xie, Z.; Bâldea, I.; Frisbie, C. D. Determination of Energy Level Alignment in Molecular Tunnel Junctions by Transport and Spectroscopy: Self-Consistency for the Case of Oligophenylene Thiols and Dithiols on Ag, Au, and Pt Electrodes. *J. Am. Chem. Soc.* **2019**, *141*, 3670−3681.
(32) Xie, Z.; Bâldea, I.; Frisbie, C. D. Energy Level Alignment in Molecular Tunnel Junctions by Transport and Spectroscopy: Self-Consistency for the Case of Alkyl Thiols and Dithiols on Ag, Au, and Pt Electrodes. *J. Am. Chem. Soc.* **2019**, *141*, 18182−18192.
(33) Li, Y.; Haworth, N. L.; Xiang, L.; Ciampi, S.; Coote, M. L.; Tao, N. Mechanical Stretching-Induced Electron-Transfer Reactions and Conductance Switching in Single Molecules. *J. Am. Chem. Soc.* **2017**, *139*, 14699−14706.
(34) Wang, K. DNA-Based Single-Molecule Electronics: From Concept to Function. *J. Funct. Biomater.* **2018**, *9*, No. 8.
(35) Bâldea, I. Ambipolar Transition Voltage Spectroscopy: Analytical Results and Experimental Agreement. *Phys. Rev. B* **2012**, *85*, No. 035442.

https://doi.org/10.1021/jacsau.6c00247
JACS Au XXXX, XXX, XXX−XXX